SAND REPORT

SAND2003-0359
Unlimited Release
Printed February 2003

A Modeling Approach for Predicting the Effects of Corrosion on Electrical-Circuit Reliability

Jeffrey Braithwaite, N. Robert Sorensen, David Robinson, Ken S. Chen and Carolyn Bogdan

Prepared by
Sandia National Laboratories
Albuquerque, New Mexico 87185 and Livermore, California 94550

Sandia is a multiprogram laboratory operated by Sandia Corporation,
a Lockheed Martin Company, for the United States Department of Energy's
National Nuclear Security Administration under Contract DE-AC04-94-AL85000.

Approved for public release; further dissemination unlimited.

Sandia National Laboratories

Issued by Sandia National Laboratories, operated for the United States Department of Energy by Sandia Corporation.

NOTICE: This report was prepared as an account of work sponsored by an agency of the United States Government. Neither the United States Government, nor any agency thereof, nor any of their employees, nor any of their contractors, subcontractors, or their employees, make any warranty, express or implied, or assume any legal liability or responsibility for the accuracy, completeness, or usefulness of any information, apparatus, product, or process disclosed, or represent that its use would not infringe privately owned rights. Reference herein to any specific commercial product, process, or service by trade name, trademark, manufacturer, or otherwise, does not necessarily constitute or imply its endorsement, recommendation, or favoring by the United States Government, any agency thereof, or any of their contractors or subcontractors. The views and opinions expressed herein do not necessarily state or reflect those of the United States Government, any agency thereof, or any of their contractors.

Printed in the United States of America. This report has been reproduced directly from the best available copy.

Available to DOE and DOE contractors from
U.S. Department of Energy
Office of Scientific and Technical Information
P.O. Box 62
Oak Ridge, TN 37831

Telephone: (865)576-8401
Facsimile: (865)576-5728
E-Mail: reports@adonis.osti.gov
Online ordering: http://www.doe.gov/bridge

Available to the public from
U.S. Department of Commerce
National Technical Information Service
5285 Port Royal Rd
Springfield, VA 22161

Telephone: (800)553-6847
Facsimile: (703)605-6900
E-Mail: orders@ntis.fedworld.gov
Online order: http://www.ntis.gov/help/ordermethods.asp?loc=7-4-0#online

SAND2003-0359
Unlimited Release
Printed February 2003

A Modeling Approach for Predicting the Effect of Corrosion on Electrical-Circuit Reliability

Jeffrey W. Braithwaite and N. Robert Sorensen
Corrosion, Electrochemistry, and Cleaning Department

David G. Robinson
Risk and Reliability Analysis Department

Ken S. Chen
Multiphase Transport Processes Department

Carolyn W. Bogdan
Component Information and Models Department

Sandia National Laboratories
P.O. Box 5800
Albuquerque, NM 87185-0889

Abstract

An analytical capability is being developed that can be used to predict the effect of corrosion on the performance of electrical circuits and systems. The availability of this "toolset" will dramatically improve our ability to influence device and circuit design, address and remediate field occurrences, and determine real limits for circuit service life. In pursuit of this objective, we have defined and adopted an iterative, statistical-based, top-down approach that will permit very formidable and real obstacles related to both the development and use of the toolset to be resolved as effectively as possible. An important component of this approach is the direct incorporation of expert opinion. Some of the complicating factors to be addressed involve the code/model complexity, the existence of large number of possible degradation processes, and an incompatibility between the length scales associated with device dimensions and the corrosion processes. Two of the key aspects of the desired predictive toolset are (1) a direct linkage of an electrical-system performance model with mechanistic-based, deterministic corrosion models, and (2) the explicit incorporation of a computational framework to quantify the effects of non-deterministic parameters (uncertainty). The selected approach and key elements of the toolset are first described in this paper. These descriptions are followed by some examples of how this toolset development process is being implemented.

Introduction

The primary mission of Sandia National Laboratories includes the responsibility for ensuring the safety and reliability of high-consequence military hardware. As such, the age-related degradation of materials used in these systems must be addressed. As shown in Figure 1, one of the most important forms of aging involves atmospheric corrosion of electrical devices. This ranking of high likelihood of occurrence with high "relative" risk (potential for undesirable consequence) is rooted in two factors: (a) corrosion has occurred in many types of fielded electrical and electronic devices (e.g., see Figure 2), and (b) a very small amount of corrosion in these devices can directly cause failure of the entire electrical circuit/system. These devices undergo corrosion damage because the two conditions required for a significant vulnerability can certainly exist: susceptible metallic materials and aggressive environments. Metals are often selected because of their electrical properties, but not their resistance to corrosion. The existence of a first-order type effect in electrical circuits differentiates this end result of corrosion from many others. That is, when a material is typically degraded by corrosion, another subsequent process causes the failure (e.g., metal thinning and mechanical overload or pitting that compromises hermeticity and permits intrusion of external contaminants). Finally, atmospheric corrosion is clearly a degradation mode that must be considered by users of electrical circuits in other types of high-reliability applications (e.g., aerospace, avionics, surveillance).

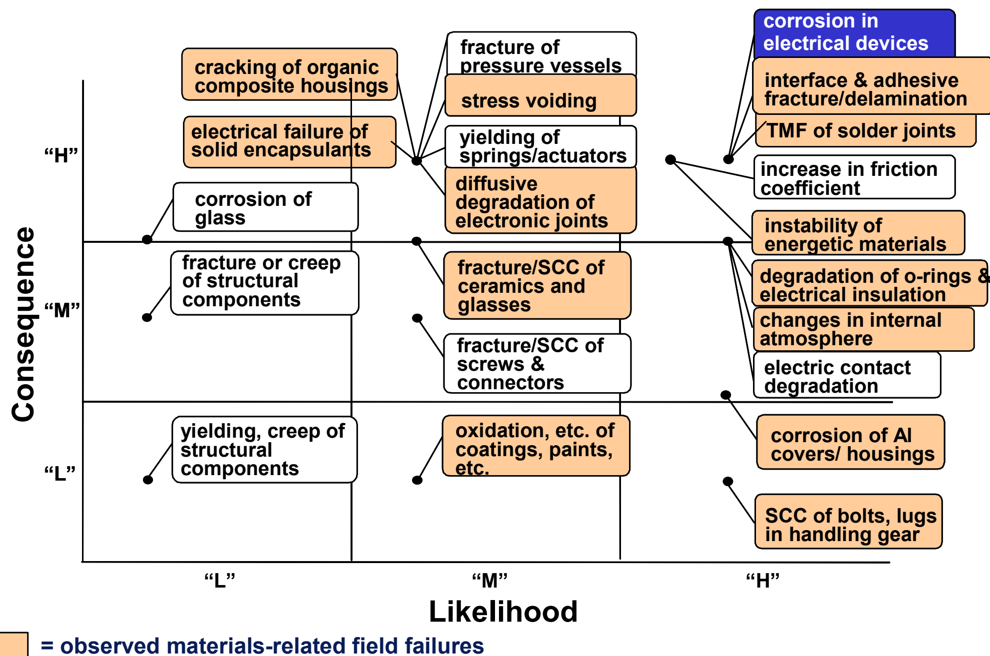

Figure 1. Compilation of the results from an assessment of likelihood of occurrence vs. potential consequence for a number of materials-degradation modes possibly relevant to high-consequence/high-reliability military systems.

Although a goal during system design is to ensure that all materials are compatible with the anticipated environment, corrosion typically still occurs because the local environment is not or does not remain as expected (e.g., a bad seal, internal material outgassing) or intended designs/configurations are not properly manufactured (e.g., wrong material, contamination). Traditionally, we have assessed the severity and potential consequences of corrosion problems that arise and then, if needed, defined remediation strategies by changing materials or implementing better control of the environment. The basis for such an assessment has normally been engineering judgment or expert opinion that utilizes historical evidence, failure analyses, accelerated aging, and, at times, limited empirical correlations. However, now

that the design and manufacturing of new systems for which Sandia has responsibility have been significantly curtailed and the desire exists to extend the service life beyond the original design goal, this traditional approach is no longer satisfactory. The new objective is to develop and employ sophisticated analytical toolsets that can predict the effects of corrosion on system performance, service life, and reliability. Such a capability will also be useful in future design activities (materials selection and environmental control). Importantly, these toolsets must be applicable to use conditions and applications currently outside of our experience base.

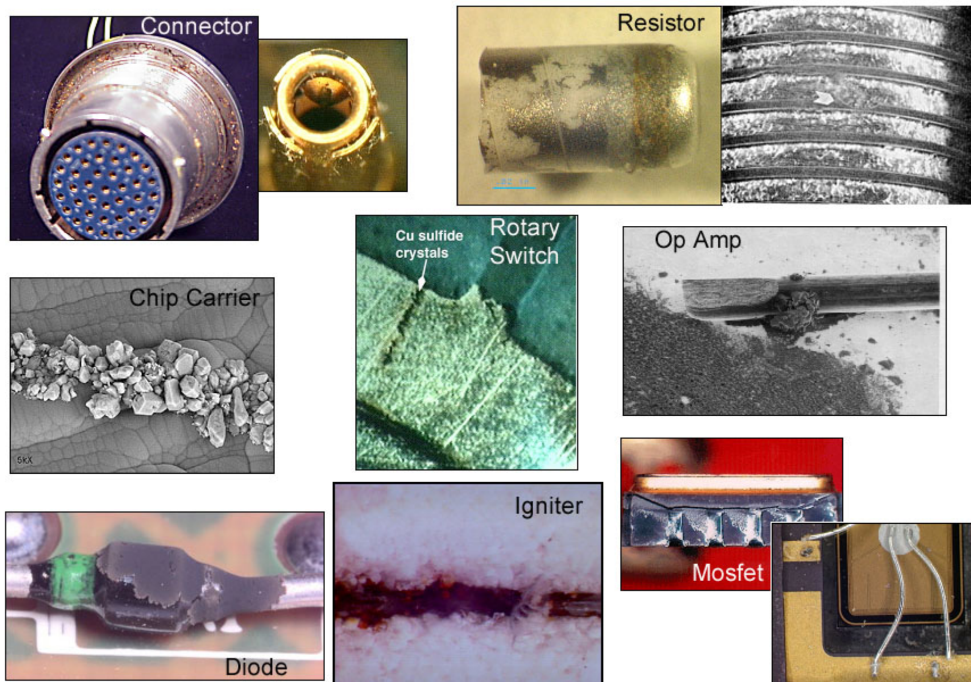

Figure 2. Photographs of some electrical and electronic devices that have undergone some form of corrosion during field deployment.

This paper is divided into two main sections. First is a description of the approach that we are following to develop such an analytical capability. The second section contains a number of specific examples that demonstrate how portions of this approach have been implemented to date along with many of the toolset attributes and development obstacles. For reference, in the remainder of this paper, the term "system" refers to any electrical circuit that has a defined function (e.g., voltage regulator, radar).

Modeling Approach

High-Level Considerations

Conventional assessments of system-level reliability are typically based on the collection of a large number of samples or observations involving failure data from both field (historical) and accelerated (stress) testing. These empirical-type analyses address the existing condition of a subject system and provide a snapshot of its reliability characteristics, but extrapolations to other hardware configurations, service conditions and lifetimes can certainly be problematic. As such, the ultimate goal for this work would be to develop a completely rigorous and robust toolset that accounts for every possible corrosion process that could occur in and all types of devices and circuits. The basic approach that would lead to this highly desirable capability is relatively straightforward. In general, it would consist of the formulation and full integration of the following four computational elements:

1. A set of deterministic mathematical models that describe how every possible form of materials degradation would affect a change in an electrical property (e.g., resistance, capacitance) of the individual piece-parts (devices) that could, either alone or in concert with others, ultimately cause system failure. Importantly, for this capability to be truly predictive, these materials models must have a physical, mechanistic basis, preferably using first principles.
2. A fully deterministic age-aware model of the performance of the entire electrical system that includes all components, devices, and interconnects. The term "age-aware" is defined in Code Complexity section below. This portion of the toolset is essential because, in general, failure (and thus reliability) can only be determined within the context of the system itself. That is, the degradation in performance of a specific device to the level that its design specification is no longer satisfied is not necessarily the same as failure at the component level. For example, it will take a very different increase in resistance of a corroding solder joint to cause failure in an RF circuit versus an analog circuit.
3. An integrating, statistical/probability-based system failure model that includes the capability to address uncertainties in process conditions and model parameters (e.g., environmental conditions, physical properties, kinetic parameters).
4. A complete, time-based definition of the expected environment (both external, internal, and micro), to include such information as use conditions, storage environments, etc.

The concurrent mathematical integration of these elements would also ensure that the myriad of possible interdependencies would be addressed. Unfortunately, because of the existence of several substantial technical obstacles (see below), the funding resources and the length of time required for achieving success with such a significant and comprehensive undertaking are simply never available. This observation is especially true when one considers that to be effective and useful in design and, in our situation, surveillance activities, the predictive toolset must really be able to assess other relevant forms of materials degradation besides corrosion (e.g., thermal mechanical fatigue, stress voiding, intermetallic growth). Some of the specific technical obstacles that impede achieving success at this rigorous level are described in the following four paragraphs.

Code Complexity

Electrical and electronic circuits can contain thousands of devices and components. Almost all available models for simulating the performance of electrical circuits are based on the SPICE code originally developed at the University of California in 1975.[1] Considering transient characteristics and mathematical convergence issues, the computational requirements for sophisticated circuits are formidable. For example, a single performance simulation of a Pentium-level IC using the personal computer version of SPICE can take two weeks to complete. This type of impediment is compounded because materials degradation processes like corrosion can only be addressed with an electrical-circuit simulator that is age-aware. That is, the calculations must be performed as a function of time with the electrical properties of each device changing as a function of time as specified by the integrated materials degradation models. In many cases, these materials models must describe multi-dimensional processes (e.g., corrosion film growth across a Au-plated copper connector surface). Then, as noted in element #3 at the first of this section, there is an absolute requirement to treat the effects of non-deterministic, distributed parameters (e.g., environmental variability, parameter uncertainty) in these simulations. Coupling all these elements together would produce an incredible "mega code." Our analysis of this situation is that the computational power to efficiently run such simulations simply does not and will not exist for the foreseeable future.

Number of Degradation Processes

There are simply too many possible failure modes in most electrical systems of interest to be able to rigorously characterize them all. For example, as listed in **Table 1**, we have estimated that there are over 20 materials degradation processes that can affect a simple printed wiring assembly. Studies at Sandia have already been directed at several of these for many years, but our understanding is still not sufficient to formulate the needed materials models.

Table 1. Examples of materials-aging processes in printed circuit board components that can cause electrical failure (typically through an increase or decrease in resistance).

Fatigue (Wires, Interconnects, TMF Solder)
Intermetallic Compound Growth (Solder Interconnects, Wirebonds, Thin Films)
Corrosion – Type I: Product Formation (Diodes, Connectors, …)
Corrosion – Type II: Voiding (Interconnects, Contacts, …)
Stress Voiding of aluminum traces (IC Interconnects)
Electromigration (IC Interconnects)
Radiation Damage (Semiconductor Material)
Diffusion In Thin Films (Adhesion Failure)
Wear / Particle Generation (Switches And Electrical Contacts)
Lubricant Degradation (Electromechanical Switches)
Electroactive Ceramic Degradation (Ferroelectrics, Varistors, …)
Magnetic Material Degradation
Insulation Degradation (Wires, Coatings, …)
Dimensional Changes (Substrates, Laminates, …)
Adhesion Degradation (Plastic Encapsulants, Conformal Coatings)
Dielectric Material Breakdown (Capacitors)
Glass And Ceramic Seal Failure (Feed Throughs, ICs, …)
Damping Material Degradation (Environmental Sensing Devices)
Diffusion In Semiconductor Materials

Physical and Device-Specific Configuration

In most situations, the length scales between the important physical processes and the dimensions of the device vary widely. As an example, consider a diode whose Cu-based braze material is undergoing sulfidation (see the photograph ahead in Figure 3). The Cu_2S precipitation reactions occur in adsorbed water layers that are < 10 nm thick. However, the film is spreading across a diode that is 4 mm long. Clearly, the sulfidation processes cannot be modeled at the nm level because millions of finite elements would be required. But even when these “sub-grid” nm processes are rolled up in constitutive equations at, for example, a µm level, convergence of the numerical solution can be achieved only when the time steps are sufficiently small. This situation could dramatically impact computational efficiency because as many as 10,000 calls may be required to a multi-dimensioned finite-element model during an extended time simulation (~ 30 years). Finally, there is the issue of the level of detail (electrical and dimensional) that is required for the physical models for each type of device that is being included. For example, over the past 20+ years, Sandia itself has used around 100,000 distinct electrical and electronic devices.

Manufacturing Variability and Changing Technology

As mentioned earlier, many of the corrosion issues that have occurred in the field are the result of improper manufacturing techniques or other unanticipated conditions (e.g., seal failure, outgassing). In reality, formulating bounds on such effects will be extremely difficult to accomplish. In addition,

component fabrication materials and technologies can change rapidly, rendering previous understanding insufficient, outdated and inaccurate.

Selected Approach

Because we believe that the development of a rigorous and comprehensive toolset that predicts all the effects of material degradation on electrical circuits is simply unattainable, we have formulated and implemented an alternative approach. This approach views the entire circuit assembly from the top down with the simple goal to efficiently allocate resources such that our confidence in the validity of the reliability prediction will be increased. In other words, system-level requirements drive the selection of which process models, device models, circuit simulations, experimentation, field data, and environmental information are included in the analysis. Inherent with the approach is the realization that this is a continuous, iterative process over the entire system life, potentially requiring multiple cycles as specific degradation modes are characterized and the system ages.

Some aspects of the conflicting needs associated with the resource decisions that have to be made are shown in Figure 3. For example, as depicted by the left arrow, the cost of acquiring reliability data typically increases with component complexity (i.e. cheaper to purchase, test and analyze discrete devices than the entire system). At the system level alone, confidence is limited because the population often cannot be properly sampled. Unfortunately, testing cannot only be performed at the materials or component level because of the increasing level of uncertainty associated with unknown effects and interdependencies. Similarly, there has been an increasing reliance on computer simulations to augment physical experimentation. However, in addition to trying to characterize the uncertainty with relevant parameters such as environment and material properties, the analysts must also account for the uncertainties introduced by the mathematical abstraction of the system. As such, proper attention to verification and validation of the computer models becomes critical.

Clearly a balance must be obtained between the information gained from testing and modeling at various levels of system indenture, the resources required to perform testing and develop models, and the uncertainties introduced in predicting system performance. The ability to logically combine information from these various areas as well as the organization, characterization and quantification of this myriad of uncertainties are critical elements of the approach being implemented at Sandia. Importantly, although the ultimate objective is to obtain accurate predictions, we recognize that real merit exists for simply obtaining more robust solutions than are presently possible (i.e. just improving our confidence in the estimates of useful life).

Primary Toolset Components

The key computational elements of our top-down development approach (schematically diagramed in Figure 4) consist of the following:

- A high-level statistical or probability-based analytical methodology.
- An age-aware electrical-system model that is mathematically decoupled from the materials-aging models.
- Computational techniques to integrate the various functional aspects within the corrosion model (including mathematically addressing parametric uncertainty).
- Baseline materials-degradation models that include the resulting effect on electrical properties and are based on the underlying physics of degradation.

Important aspects (along with definitions of the terms used in this figure) for the each of these components are discussed in the following subsections. Importantly, the output from the integrated corrosion portion of the toolset enables circuit reliability to be determined as a function of time.

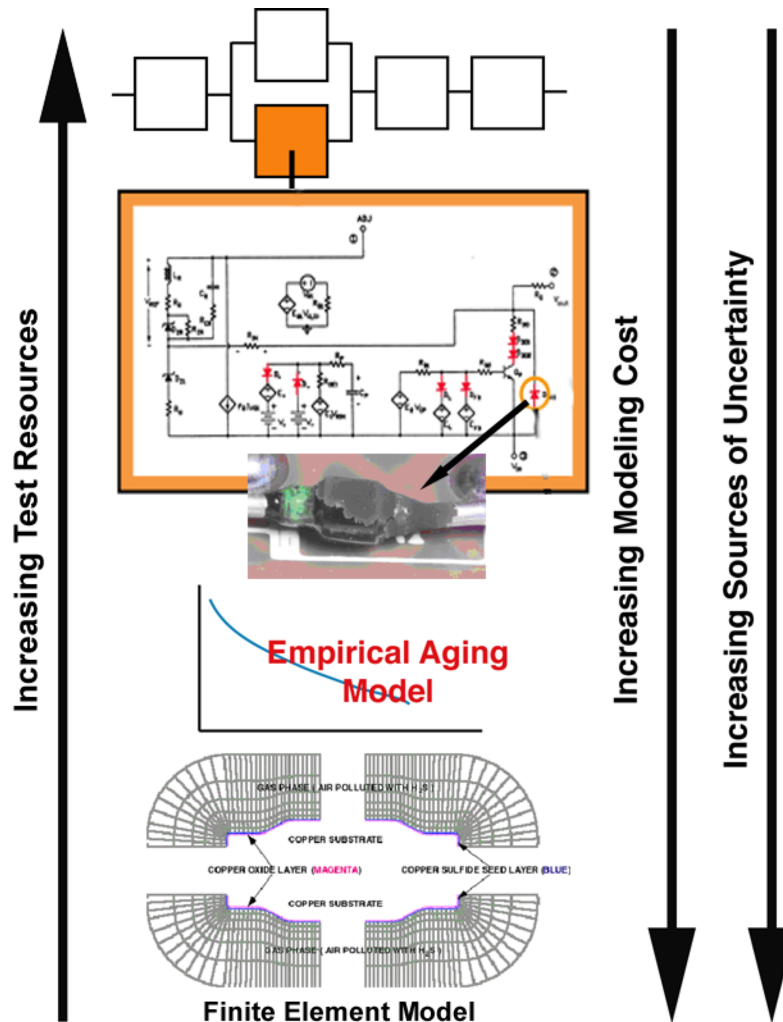

Figure 3. Conflicting objectives of modeling detail, testing resources and uncertainty in predicted system performance. The example involves a 4-mm zener diode in which a copper-containing braze sulfidized. The resulting Cu_2S spread across the surface. The finite-element representation of the geometry of this corrosion process is also shown.

Analytical Methodology

Based on an assessment of several alternatives, the decision was made to incorporate Bayesian statistical techniques into the system-level analytical framework. This methodology was selected primarily because of its ability to improve the efficiency of the iterative development process.[2,3] This advantage is gained because of its required system perspective, the effective use of sensitivity studies and engineering judgment, and the direct mathematical incorporation of information from many different types and levels of sources (e.g., system, sub-system, component, device). Specifically, hierarchical Bayesian methods are particularly suited to this latter capability in that relationships between test articles can be explicitly included in the analysis.[4] Classical Bayesian methods assume that the articles under test are not related in any manner even though the articles may be identical.

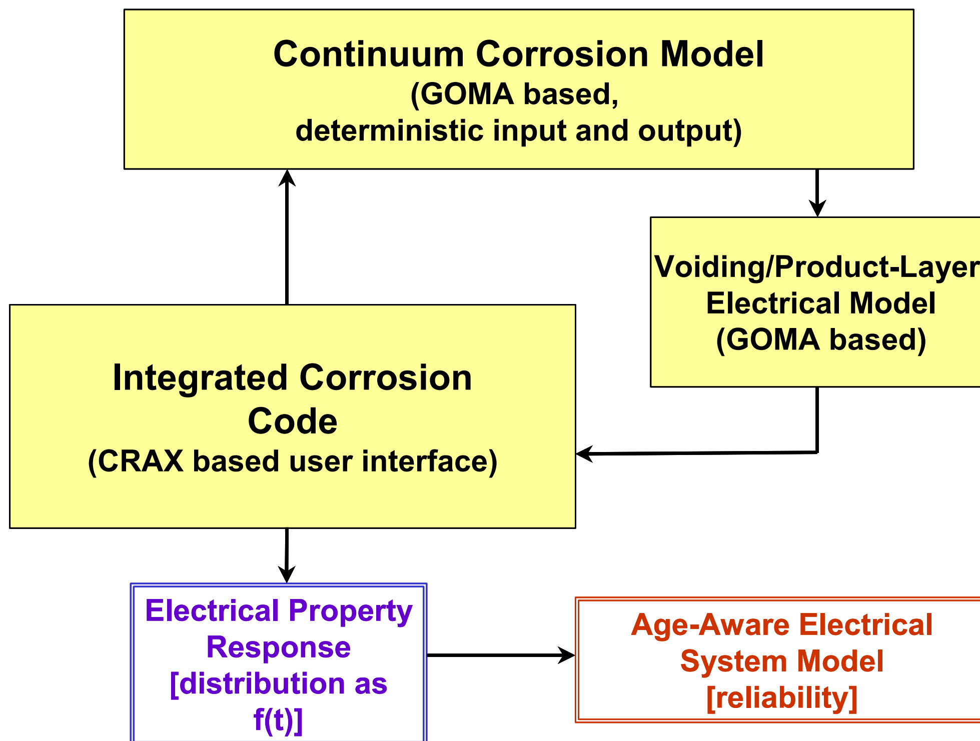

Figure 4. Information flow diagram for the various elements of a mathematical toolset that permits the prediction of the effects of corrosion on the reliability of electrical circuits. GOMA is the name of a multi-dimensional, finite-element code that is used to simulate the corrosion processes and CRAX is one of the codes used to include uncertainty in the analyses (both discussed below in more detail).

In particular, the use of this more modern methodology will permit relevant expert opinion, materials aging, field reliability data, and laboratory failure data to be codified and merged. For example, if laboratory experiments and detailed mathematical simulations are too expensive, empirical models based on data from field measurements and/or component/subsystem testing can drive model refinement. In addition, this methodology has the capability to address both failures due to aging effects and random failures due to unaccounted for latent defects.

Specifically in this process, initial estimates of how corrosion affects service life are formulated primarily using expert opinion and engineering judgment. This paper-type study effectively replaces the first stage of model-development activities (#1, #2, and part of #3) defined above under High-Level Considerations. The resulting and typically empirical equations obtained by this method are input into some level of electrical circuit/system model. The apparent sensitivity of the system service life to specific materials degradations can then be determined. This type of system-level analyses provides more quantitative understanding about which types of materials aging processes probably contribute most strongly to system failure. Additionally, the sensitivity study results are coupled with additional expert opinion to improve the initial model formulations. This information is then analyzed to identify aspects of materials aging where an enhanced definition/quantification would provide optimal benefit at minimal cost. To aid the model refinement process, results from accelerated-aging studies at the device/sub-system level can be used in conjunction with traditional field failure data.

Critically, resources must be focused into very selected and specifically identified areas to develop the mechanistic or “physics of failure” basis required for a truly predictive capability. These “materials

physics" models incorporate an understanding of the materials/property relationships that include the quantification of the kinetics of chemical and microstructural changes in the material, and functional dependencies on extrinsic environmental parameters such as temperature and humidity. The information produced by the materials-physics models is combined with data from a broad range of related sources including (1) experimental results from the literature and previous investigations, (2) laboratory materials experiments, (3) laboratory "device level" testing, and (4) historical field-failure data from relevant subsystems with similar designs. This collective knowledge base is then used to refine and improve the initial "skeleton" model and this process is iteratively continued. Often, the translation from the materials physics model to the improved skeleton model requires higher-level electrical simulations and/or the inclusion of expert opinion.

Importantly, if this type of iterative refinement loses focus, the process will tend back towards the rigorous solution and thus the development process will become unacceptably costly and time consuming. To avoid this situation, significant attention must be paid to keep the scope and detail of the material model refinement to a minimum by performing frequent iterations with the system-level model. That is, the system level model will be used to reveal the changes in (system) sensitivity after the new (skeleton) models are employed.

Electrical-System Model

As stated earlier in this section, most of the commercially available electrical-circuit simulators are based on the UC Berkeley SPICE code. A good overview of the foundation of this program, its popular variants, and its basic operation is available at the URL listed in Reference 1. Basically, SPICE is a general-purpose circuit simulation program for nonlinear dc, nonlinear transient, and linear ac analyses. Circuits may contain resistors, capacitors, inductors, mutual inductors, independent voltage and current sources, four types of dependent sources, lossless and lossy transmission lines (two separate implementations), switches, uniform distributed resistor-capacitor lines, and five of the most common types of semiconductor devices. At Sandia, we routinely use the PSPICE code from MicroSim Corp. that runs on personal computers and two Sandia-developed codes: ChileSPICE (based on SPICE version 3F5) and XYCE (pronounced zice). The primary enhancement relative to PSPICE that ChileSPICE includes is the capability to run the simulations with parallel processors. This capability can significantly reduce computer execution times. For example, with complex circuitry, run times can be reduced by factors of 25 or greater. XYCE just recently became operational. It is a code that was developed from scratch with efficient parallel processing, improved solvers, and distributed memory as prime design criteria. All three codes are now used in age-aware simulations – that is, the ability to perform the electrical simulations as a function of time has been incorporated. Currently, these age-aware calculations are normally performed in a "static" fashion in which the time is advanced simply by including the electrical properties of the various constituent devices consistent with the selected age. Thus, no interdependencies of the aging process between devices and components are presently addressed.

To enable the circuit simulation codes to be able to address corrosion, two modifications must be performed. First, electrical elements must be added to the base electrical circuit that will account for the effects of corrosion. Such a modification is shown in Figure 5 for the corrosion of three wirebonds used in the packaging of a simple LM185 voltage reference device. Here, a resistor has been added in series with each of the wirebonds that permits the increase in resistance due to corrosion to be included. The second requirement is to decouple the corrosion model from the electrical circuit model to improve computational efficiency (issue discussed above). This goal is achieved by having the corrosion model calculate a time-based change in an associated electrical property (e.g., for this situation, the series resistance for each of the wirebonds). As corrosion proceeds, the resistance increases. This output (in the form of a look-up table or empirical equation) can then be used directly in the electrical circuit simulator.

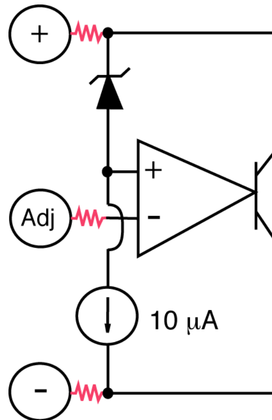

Figure 5. Schematic diagram of an LM185 voltage reference device showing the three resistors that were added to simulate the effect of wirebond corrosion. The values of the resistors increase time.

Uncertainty Analysis

As stated earlier, the explicit inclusion of the capability to address uncertainties inherent in many material properties and the operating environment is a critical toolset element. To properly illustrate this need, consider the simple case of a device containing a single wirebond that is susceptible to corrosion. Figure 6 shows a hypothetical curve of resistance as a function of time for such a device. The resistance increases gradually with time as corrosion proceeds. At some time, a critical resistance is reached, and the device will no longer function as intended. A straightforward deterministic calculation would yield a service-life prediction indicated by the vertical line farthest out in time. However, if the uncertainty in the parameters (that always exists at some level in real situations) is included in the analysis, a distribution of predicted resistance values can be calculated at each time. The tail of each distribution that is above the critical resistance represents the probability of failure at that time. In this case, by the time the deterministic service life is reached, the reliability will be lowered to 50%. In high-reliability systems, risk of failure may become unacceptable when only a small tail of the distribution exceeds the critical resistance (as shown in Figure 6). Very importantly, the failure criteria for each wirebond in a device will, in general, be different for each specific type of application. Therefore, the output from the integrated corrosion model must consist of a time-based distribution of changes in electrical properties (e.g., wirebond resistance values) and not a failure probability.

To simultaneously include the variety of distributed parameters associated with real system knowledge into the deterministic corrosion-process models, two different Sandia-developed software packages are used: DAKOTA and CRAX. These codes not only include advanced uncertainty analysis engines, but as will be demonstrated, also serve an integrating function for the overall corrosion model (see Figure 7). For illustrative purposes, in the remainder of this paper only CRAX will be discussed.[5] The uncertainty analysis engine within the CRAX package is termed Cassandra. Cassandra's efficiency is very important because it directly impacts the number of required calls to the deterministic corrosion process model. For example, a typical "Monte Carlo" analysis might require 30,000 or more calls to the corrosion-process models per time step. Newer techniques such as Latin Hypercube sampling (LHS) might reduce this requirement to around 500 calls. The advanced techniques used in Cassandra may only require 50-100 calls and include LHS, quasi-Monte Carlo (qMC), advanced mean value with fast probability integration (AMV/FPI), and a new method referred to as the Field Analysis Method (FAM).[6,7] If the process models are multi-dimensional, finite-element based (as in our situation with GOMA), such efficiency is a critical factor.

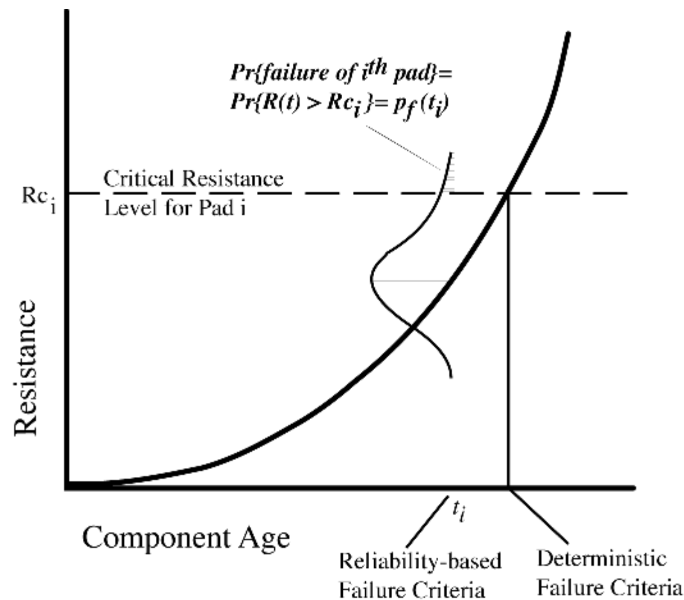

Figure 6. Plot of a hypothetical change in wirebond resistance to demonstrate how the existence of uncertainty permits the probability of device failure to be calculated (shaded area under the tail of the distribution).

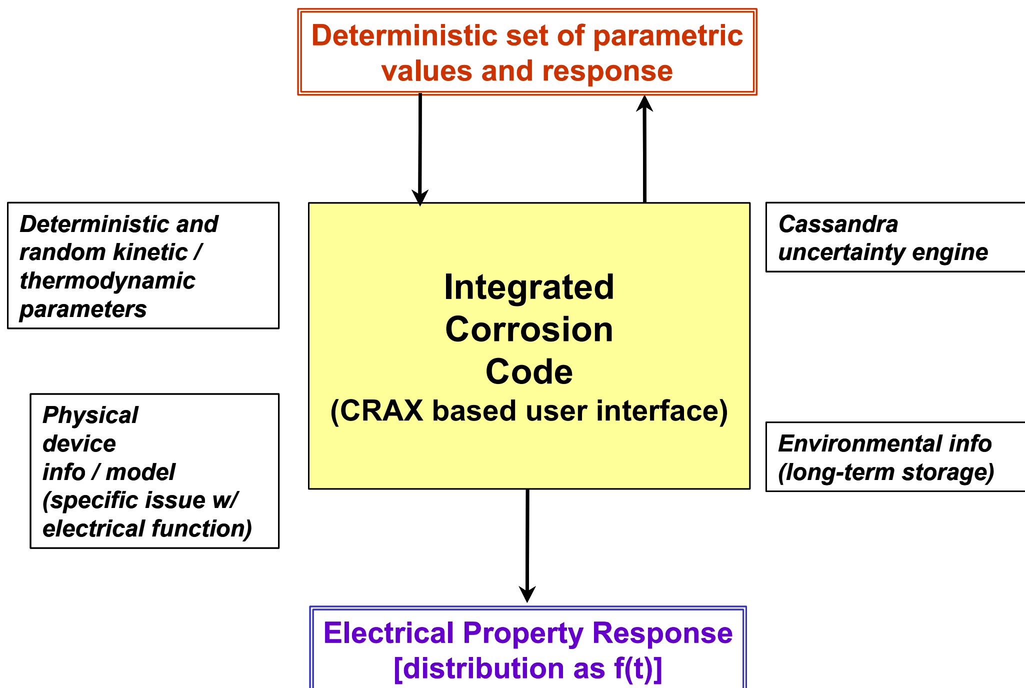

Figure 7. Information flow for the integrating, parameter sampling and uncertainty analysis function of the corrosion code.

The computational framework of the actual simulations that produce the desired output (change in electrical property) follows a relatively straightforward path. First, a value for each of the non time-based distributed parameters (e.g., rate constants) is sampled by CRAX and fixed. Next, distributions for each of the time-based distributed parameters (e.g., temperature and humidity) are sampled for the first time step and the governing physical models within GOMA are called and numerically integrated to produce a deterministic estimate of the property change. As is described in more detail below, GOMA is a multi-

physics, multi-dimensional, finite-element computer code with massively parallel processing capabilities. It was developed and is currently being enhanced at Sandia. Then, new parametric values for the distributed parameters are sampled consistent with the time step, the deterministic governing equations are again solved, and the property change due to corrosion is accumulated. This process is repeated until a pre-specified length of aging has been achieved, effectively yielding a simple time-based property response for a single device. This entire process is then repeated for a number of other devices with the actual number of simulations required being dependent on the uncertainty analysis technique being used within CRAX. Compilation of all the responses at each time step produces the desired distribution.

The exchange of information between CRAX, Cassandra, the physical corrosion model (GOMA in this situation), and even ChileSPICE can follow many paths. Within CRAX is the capability to either recompile the existing software into the Cassandra engine, thereby significantly increasing computational efficiency, or rely on 'hand-shaking' between the CRAX, the Cassandra engine and the existing GOMA software (see Figure 8). The former approach was adopted in the age-aware reliability simulations described in the implementation section of this paper. The CRAX interface with the other networked elements can easily be modified to handle either of these options. In addition, Cassandra is platform independent and complies with the Common Object Request Broker Architecture (CORBA), providing an effective interface with many of the new engineering design and analysis software packages.[8]

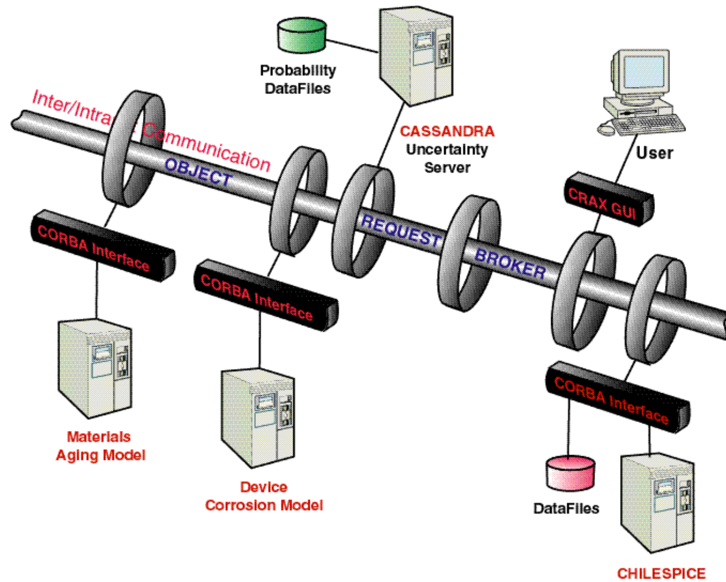

Figure 8. Diagram depicting the networking relationships of the various elements associated with the corrosion toolset.

Corrosion Process Models

The core of the desired predictive toolset consists of deterministic physics-based models of the relevant corrosion processes. Some of the computational efficiency and complexity considerations that must be taken into account in the formulation of these models were discussed earlier. They include the large number of physical and chemical processes that are involved in corrosion reactions, the differences between device and process length scales, the large number of required computations that often will be multi-dimensional, and the need to include moving boundaries. This moving-boundary aspect is a very non-trivial computational challenge that is caused by the dynamic growth or voiding of the corrosion processes (e.g., growth of Cu_2S product layer). Some of these factors are obvious from the photograph and the finite-element mesh shown earlier in Figure 3. Taken together, these factors force the employment of continuum-level models in which the real mechanistic processes occur at a length scale much smaller

than that associated with any finite elements used (termed sub-grid). The Sandia-developed GOMA code is currently being enhanced to address the relevant gas-phase, liquid phase, and solid-state transport processes as well as heterogeneous electrochemical reactions associated with corrosion. For the corrosion application, the flow of information to and from GOMA is depicted in Figure 9.

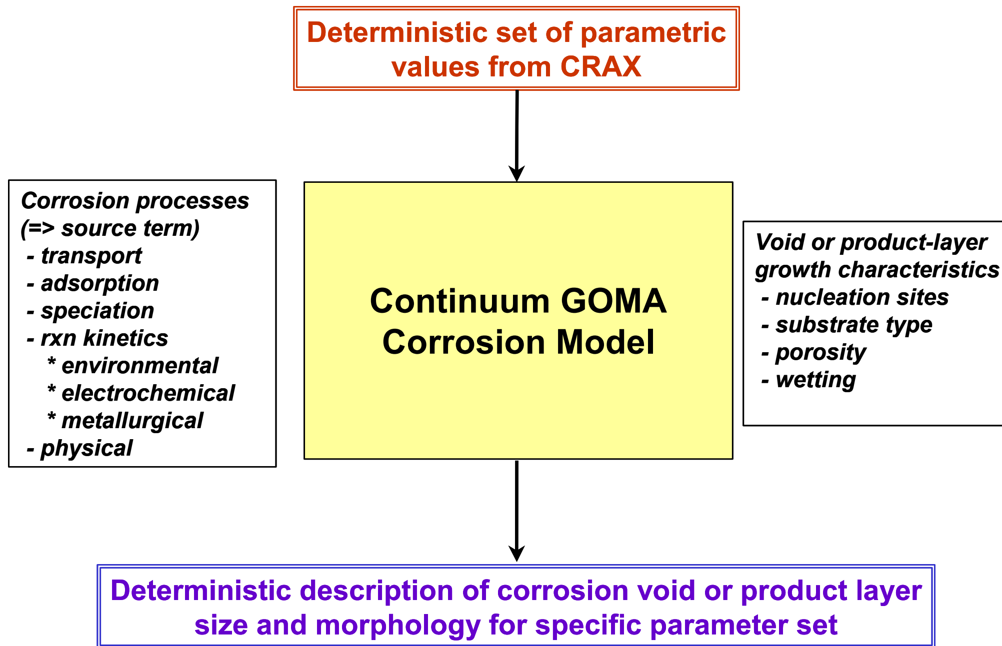

Figure 9. Information flow for the deterministic corrosion model using the GOMA finite-element computer code.

Implementation of the Selected Approach

Although the identification of a high-level process to develop the desired analytical capability is relatively straightforward, achieving success certainly is not. The formidable nature of this activity is the result of several factors including the “soft” reliance on expert opinion (not receptive to rigorous analysis), the existence of a wide range of diverse requirements that must be incorporated, and the need for the toolset to have a very computationally efficient framework. Primarily because our level of expert opinion and our mastery of the Bayesian statistical approach has not been adequate to establish the first skeletal model, our decision was to select some relevant corrosion degradation modes that have been observed in our hardware and use them as initial “development” vehicles. In other words, for this initial stage, we chose to develop our understanding of the various toolset elements and how they link together using two specific types of observed corrosion: the sulfidation of copper-containing features (e.g., in diodes, contacts, connectors) and voiding in thin-film aluminum (e.g., wirebonds contained in integrated-circuit packaging). As will be shown, this work has facilitated the advancement of our approach and has clearly demonstrated the ultimate usefulness of the toolset.

In the following discussion of our progress, we start at the bottom (gaining of scientific understanding) and progress through to a full reliability simulation of an electrical circuit. Therefore, the following subsection describes how a continuum-level deterministic corrosion model is formulated and then used to compute a change in an electrical property (essentially addressing the toolset elements shown previously in Figure 9 plus the upper right element in Figure 4). Next, two different examples are presented of how these types of deterministic models are subsequently used to calculate the impact on electrical circuit reliability. The important elements added in these latter cases are the analysis of

uncertainty and the link with age-aware electrical circuit simulation models. There is an important aspect of this presentation that should be kept clearly in mind when reading the remainder of this paper: although some level of detail is included in these analyses, the intent here is to communicate how this approach can be implemented and, again, to show its system-level value. As such, to minimize distraction from this objective, many specific assumptions and explanations of phenomena are not included.

Deterministic Corrosion Model

The physical/scientific base for an effective predictive capability must be contained in the deterministic and mechanistic process models. These models must capture the essential phenomena that occur in the corrosion processes, which necessarily employ all of the relevant parameters that influence the corrosion processes. Incorporation of these parameters can be either explicit or implicit through sub-grid parametric combination (discussed in more detail below). The output from the deterministic models is the effect of corrosion (e.g., product layer growth or voiding), which is subsequently converted into a change in a relevant electrical property as a function of time. As noted in the previous section, because of the necessity to calculate effects on devices that have finite dimensions, computational considerations force us to consider performing the deterministic modeling only at the continuum level. Therefore, one of the primary activities involves formulating proper governing constitutive equations for each important corrosion process at the sub-grid level.

For this discussion, the degradation of an electrical contact was chosen. Although not universally true, experience with our systems has shown that when copper and silver metallization features corrode, they typically are sulfidized to form Cu_2S or Ag_2S. Therefore, in this simplified example, degradation of the contact occurs by sulfidation of copper through pores in the gold plating. The objective then is to address the effect of the growing Cu_2S film on the resistance of the electrical contact. The main purpose of this subsection is to describe our initial effort to develop a reasonable and appropriate deterministic corrosion model.

Constitutive Equations

Copper Sulfidation

For a gold-plated contact, sulfidation of the underlying copper layer results in the build-up of corrosion products on the surface. The reaction is possible wherever there are pores in the Au (and Ni interlayer), exposing the Cu substrate. The chemical reaction of the Cu with the H_2S-containing environment is the same, regardless of the presence of the Au layer, although the kinetics may certainly change due to the limited exposed Cu surface area, water adsorption phenomena and possibly galvanic effects. Overall, copper sulfidizes in H_2S according to the following reaction:

$$H_2S + 2Cu + \tfrac{1}{2}O_2 \rightarrow Cu_2S + H_2O \qquad (1)$$

The kinetics of the reaction are affected by the ambient environmental conditions (temperature, O_2 and H_2S partial pressures, and relative humidity) and by physical properties (e.g., Cu^+ and H_2S diffusivity).[9] To formulate the constitutive equations needed to describe these effects and the physico-chemical processes ongoing during the sulfidation of an electrical contact, two levels of experimental studies were performed. In the first series, the sulfidation kinetics of bare copper were characterized. The results provided information relative to the intrinsic rate of sulfide-product formation (the source term). In the second series, sulfidation of Au plated Cu coupons was studied, providing information on the effect of the Au plating and the resulting product-layer morphology and growth kinetics.

Graedel and co-workers earlier showed that growth of copper-sulfide films occurs in two distinct stages (see Figure 10a).[10] They proposed that Stage-I was controlled either by a surface reaction or by

gas-phase mass transport and Stage-II by diffusion of cuprous ions through the thickening product layer.[11] To better quantify the actual rate-controlling process, sulfidation kinetics were measured and mathematically modeled using a reactor configuration that has well-defined flow characteristics and which minimizes the potential for gas-phase mass transport control.[9] The significant findings from our kinetic sulfidation experiments include the following:

- Initial (Stage-I) kinetics are linear and first-order with respect to the concentration of H_2S in the gas phase [H_2S] up to relatively high levels of about 200 ppb (Figure 10(b)).
- Stage-I rate is controlled primarily by gas-phase mass transport at higher relative humidity (RH) levels, but evidence exists of partial surface reaction control at lower RH levels. The activation energy for this stage in low humidity conditions is consistent with mixed kinetic control (6.3 kcal/mole). As a side note, the confirmation of Graedel's original suggestion that Stage-I could be controlled by gas-phase diffusion may be very important in that it might explain the wide variation in reported rates of copper sulfidation.
- Stage II has a relatively parabolic shape and is observed primarily at mid to high humidity levels (Figure 10(a)).
- Stage II is controlled by Cu^+ ion vacancy transport through the Cu_2S product layer (diffusivity measured with marker experiments to be 10^{-15} cm^2/sec).

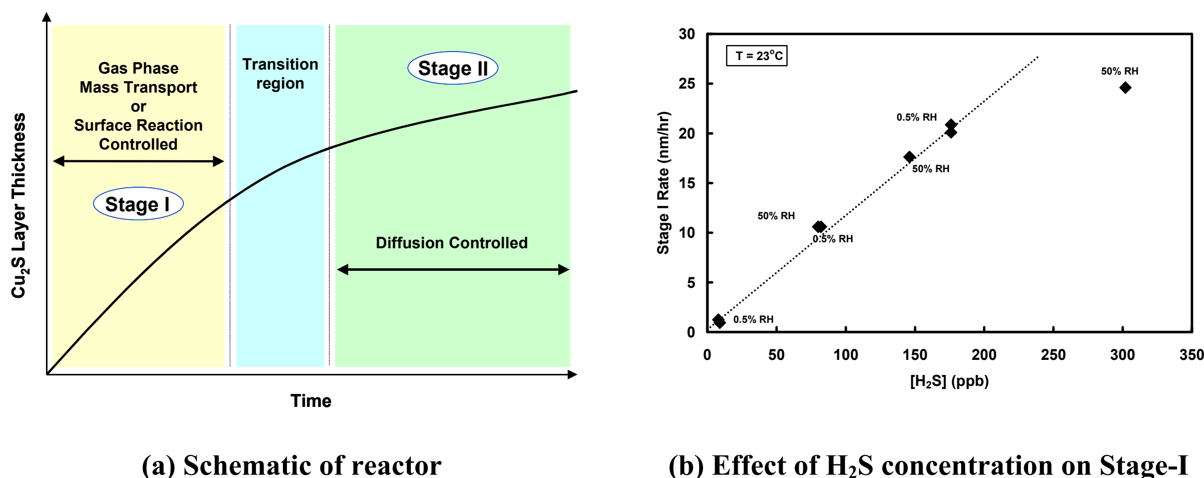

(a) Schematic of reactor **(b) Effect of H_2S concentration on Stage-I**

Figure 10. Selected results from copper sulfidation kinetic studies: (a) schematic diagram showing two stages of sulfidation kinetics, and (b) the linear relationship of Stage-I rate on [H_2S] up to about 200 ppb.

At the present time, the effect of the galvanic coupling with the noble gold plating layer has not been quantified. As such, the factors that are available for inclusion in our equations describing the copper sulfide growth rate include the exposed surface area of the copper (through the gold pore), temperature, [H_2S], humidity, surface reaction rate constant for Stage-I, and Cu^+ ionic (really copper vacancy) diffusivity through the Cu_2S product layer for Stage-II.

A schematic diagram of the important phenomena associated with copper sulfidation is shown in Figure 11 (left). This figure shows the Cu, Cu_2S, adsorbed water and gas layers and depicts the important processes that occur in each layer. In the gas phase, H_2S is in equilibrium with H_2S dissolved in the adsorbed water layer. Oxygen is reduced at the sulfide-water interface and Cu is oxidized at the Cu-Cu_2S interface. Cuprous vacancy (Cu^+) and electron hole (e^-) transport through the sulfide layer is required for film growth and to preserve electrical neutrality. Copper sulfide is formed through a reaction between Cu^+

and $S^=$ at the copper sulfide surface. Using our collective knowledge and available experimental data, the governing constitutive equations (shown in Figure 11, right) were formulated. A more detailed compilation of our understanding of these processes is contained in Reference 9. Also of note and as discussed in the previous section, the disparity between the length scale of the corrosion processes and the size of the macroscopic devices (e.g., contact or diode) prevents the explicit inclusion of some of this process understanding. For example, the adsorbed water and the original copper oxide is only about 3-5 nm thick. As such, computational limitations force the knowledge of these micro- to meso-scale processes to be included in lumped kinetic and property parameters (e.g. surface rate constants & diffusion coefficients) at the sub-grid level.

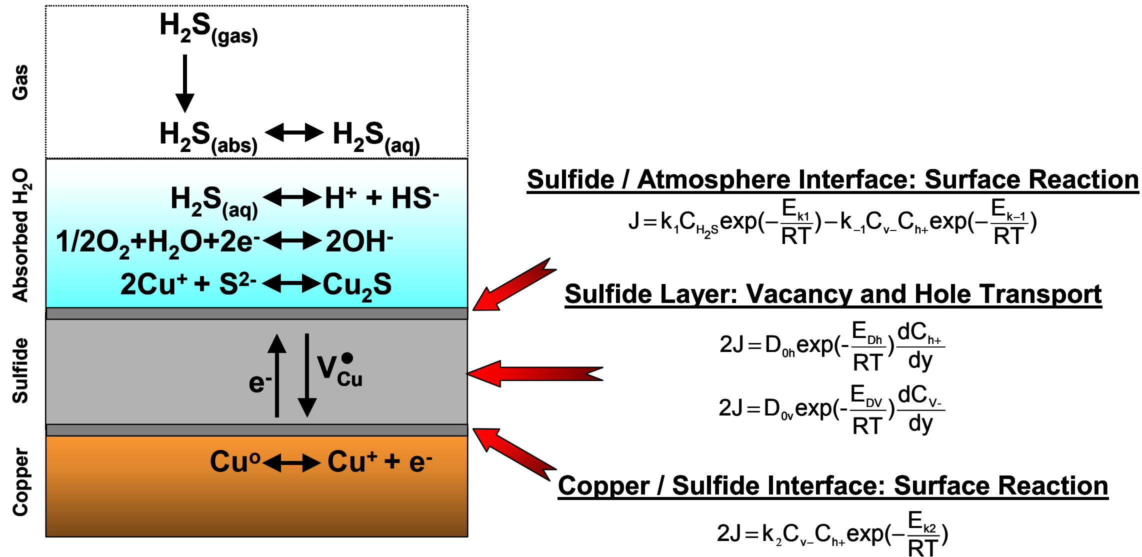

$$J = k_1 C_{H_2S} \exp(-\frac{E_{k1}}{RT}) - k_{-1} C_{v-} C_{h+} \exp(-\frac{E_{k-1}}{RT})$$

$$2J = D_{0h} \exp(-\frac{E_{Dh}}{RT}) \frac{dC_{h+}}{dy}$$

$$2J = D_{0v} \exp(-\frac{E_{DV}}{RT}) \frac{dC_{v-}}{dy}$$

$$2J = k_2 C_{v-} C_{h+} \exp(-\frac{E_{k2}}{RT})$$

Figure 11. Schematic diagram of the copper sulfidation process showing the important phases and interfaces. The governing constitutive equations for the relevant processes are listed on the right.

Electrical Contact Resistance

This subsection describes how the nonlinear and coupled governing equations for the deterministic continuum corrosion model are numerically solved using the GOMA code. The situation being addressed is an intermittent electrical contact that is exposed for an extended time period in a relatively high-humidity, sulfidizing environment. In this case, the output from the GOMA computations is the change in the resistance of the contact. Under the assumed conditions, the reaction is in a Stage-I regime for only a brief period of time. The majority of the copper sulfidation occurs in Stage-II where solid-state copper-vacancy diffusion in the Cu_2S product layer is rate limiting. For these simulations, a slightly simplified set of constitutive equations from those presented in Figure 11 was solved. Here, a first-order surface reaction was coupled to Fick's second law of diffusion. The resultant equation that describes the concentration of cuprous copper ions within the Cu_2S corrosion product was solved in GOMA along with those equations that account for mesh motion caused by the dynamic growth of Cu_2S at the moving Cu_2S/gas interface. The boundary conditions used for solving the Fickian diffusion equation included: a) at the moving sulfidizing surface, the species diffusion flux is equal to the simplified first-order rate of sulfidation; and b) at the Cu/Cu_2 interface, the concentration of cuprous copper ions is taken to be constant and equal to its initial value in the thin seed layer, which is used to initialize the finite-element computation. Moreover, the contact angle between the copper sulfide and the substrate (e.g. gold) was specified and it served as a boundary condition for the mesh-motion equations so that the geometry at the Cu_2S/substrate contact line can be determined. Lastly, remeshing (generation of new finite-element mesh)

and remapping (mapping solution variables from old mesh to new mesh) are performed repeatedly to maintain the average size of the mesh employed and thus reduce solution inaccuracy. Once concentration of cuprous copper ions within the Cu_2S domain is known (by solving the governing equations), sulfidation rates were readily computed using the simplified first-order surface-reaction rate expression.

As soon as the growing domain of the copper-sulfide corrosion product is determined by solving the equations governing Cu^+ diffusion and mesh motion, the electrical potential field within a pin-Cu_2S-pad electrical contact assembly can be computed by solving Poisson's equation that describes charge conservation with electroneutrality valid everywhere within the electrical contact assembly:

$$\nabla \cdot (-\kappa \nabla \Phi) = 0 \tag{2}$$

where Φ is the electrical potential in volts and κ is the electrical conductivity (a function of material composition in the electrical-contact assembly). Once the electrical potential is known, the total electrical current being conducted through the assembly, I, can be readily computed from:

$$I = \int (-\kappa \nabla \Phi) dA . \tag{3}$$

The integral above can be evaluated using a conveniently chosen cross-sectional plane, e.g., at either end of the assembly. Finally, the effective electrical resistance of the assembly, R, is numerically calculated within GOMA by using Ohm's law:

$$R = \frac{\Delta \Phi}{I} = \frac{1}{\int (-\kappa \nabla \Phi) dA} \tag{4}$$

Several GOMA-based simulations were performed to demonstrate the linkage between the copper sulfidation reaction and its effect on increasing the resistance of an intermittent contact. For these calculations, the assumption was made that a defect in the gold plating exists immediately under the contact area and, again, that high humidity conditions exist. Figure 12 and Figure 13 show the predicted shape of the copper-sulfide product within and outside the pore, respectively (function of time). Comparing the shape of the calculated corrosion "bloom" shown on the left side of Figure 13 with that observed in a cross section of an actual bloom (right side), the simulated shape is somewhat approximated. Importantly, the colors in the copper sulfide region in Figure 12 and Figure 13 are indicative of the concentration contours of the cuprous copper ions. The parameters used in these computations include: vacancy diffusivity – 10^{-15} cm^2/s, first-order rate constant – 10^{-9} cm/s, concentration of initial cuprous copper ions in the seed Cu_2S layer – 1 $mole/cm^3$, and Cu_2S/substrate contact angle – 90°.

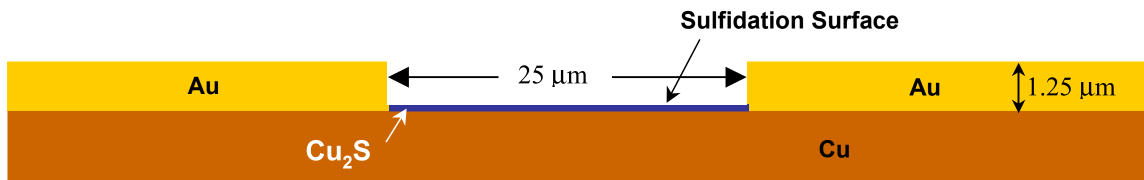

Figure 12. Predicted growth of copper sulfide within the 25 µm pore at time ~ 3 days.

Numerical solutions to Equations 2-4 yielded predicted contours of electrical potential within the pin-Cu_2S-pad contact assembly at an extended time period of >20 years (Figure 14). The colors represent bands of equal potential. Note that the large rectangular structure at the top of this figure represents the electrical contact and the Cu_2S corrosion product is the banded structure near the bottom. As shown, this Cu_2S mound was taken to be deformable and the contact interface conforms to the rigid flat surface of the gold-plated copper pin. As shown in Equation (4), the increase in contact resistance due to the presence of the copper sulfide is linearly dependent on its electrical conductivity. In these simulations, a value of 1

$(\Omega\text{–cm})^{-1}$ was used. Conductivity measurements reported in the literature range from around 0.07 to 1 $(\Omega\text{–cm})^{-1}$ for Cu_2S.[12] The result from this deterministic simulation was that the electrical resistance of the contact assembly would increase to about 5 ohms due to the presence of this 10 µm Cu_2S layer.

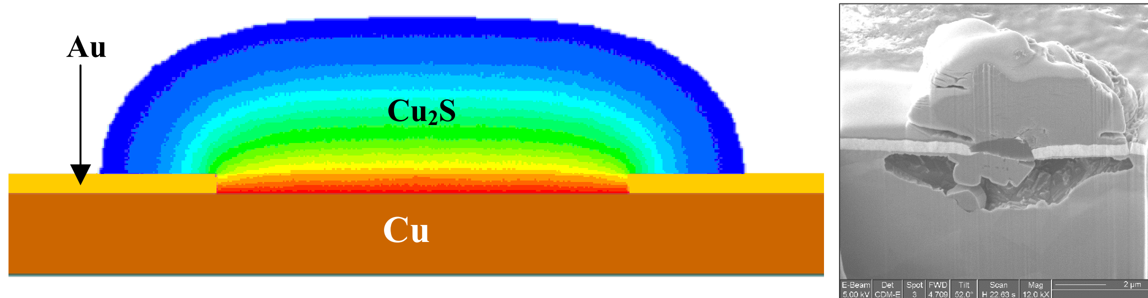

Figure 13. Predicted growth of copper sulfide outside the 25 µm pore at time ~ 5 years (left) and a cross-section view of a copper-sulfide mound that formed over a gold pore (right). The lighter material that is on the top of the mound is platinum that was added to help the ion-beam sectioning of the sample.

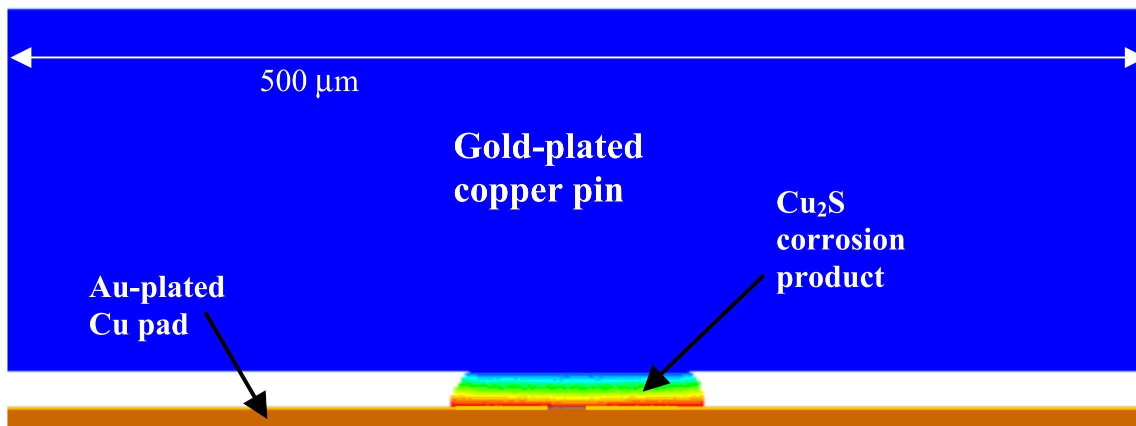

Figure 14. Predicted electrical potential contours in the pin-Cu_2S-pad electrical contact assembly.

Integrated Corrosion Model

This section describes our progress relative to including uncertainty in the toolset and interfacing the results with age-aware electrical system models. Two examples are presented. The first one involves the sulfidation of a diode and is included for two purposes: (1) to show how the existence of uncertainty has been incorporated into the analysis, and (2) to demonstrate that, in some situations, a full coupling with the age-aware system model is not needed to produce desired circuit reliability information. The second example addresses corrosion of aluminum wirebonds in two plastic-encapsulated microelectronic (PEM) devices. This latter topic is included to demonstrate a full implementation of the toolset. Both of the following descriptions follow a similar format: development of constitutive and deterministic governing equations, incorporation of uncertainty, and a determination of the effect of the corrosion on the long-term reliability of the circuit.

Diode Sulfidation

During fabrication of an electrical component, several zener-type diodes were found to contain layers of copper sulfide on their outer surface (see photograph in Figure 3). An investigation was performed that led to the finding that the copper in a braze material used within the diode sulfided during long-term

storage. The sulfiding agent was an organic sulfide species (RSH) that off-gassed from rubber bands. These bands were used to package several diode together during storage. The Cu_2S film initiated at pores in the epoxy body near the diode ends and spread across the surface. In some instances, the Cu_2S layer was extensive enough to cause unacceptable reverse-bias shorting of the diode between the leads.

A series of deterministic equations was first formulated to describe the sulfidation process. A continuity equation addressed the mass balance of the off-gassing sulfide species in which the accumulation of sulfur species in the vapor space is determined by the difference in the rates of production (outgassing) and consumption (Cu sulfidation):

$$\frac{dQ_v}{dt} = \frac{dQ_{rb}}{dt} - \frac{dQ_{sr}}{dt} \tag{5}$$

where Q denotes quantity, *v* is vapor space, *rb* is the rubber bands, and *sr* is sulfidation reaction occurring on the diode surface. Once Q_v is determined by analytical solution of the above equation, the copper sulfide (*cs*) production rate (source term) can be calculated using the following equation:

$$R_{cs} = \frac{dQ_{cs}}{dt} = \frac{5k_{sr}\varepsilon}{vol} Q_v = 5k_{sr}\varepsilon[RSH] \tag{6}$$

where k_{sr} is the surface-reaction rate constant, ε is the porosity of the epoxy on the diode and [RSH] is the concentration of gaseous sulfur species in the atmosphere above the diode. The formulation of this equation is an example where expert opinion was used. That is, the assumed first-order dependency on ε and [RSH] was based on observed copper sulfidation kinetics (as noted above) and on the probable effect of porosity on exposed surface area. Values for the rate constants were estimated from different aspects of the diode sulfidation information obtained after storage along with results from focused coupon-type accelerated aging studies. Solving these constitutive equations yields the quantity of Cu_2S formed as a function of time (source term).

Based on visual and SEM observations of actual devices and again on specifically designed aging studies, the sulfide layer was assumed to grow across the diode surface in a predictable manner with the following characteristics:

- The corrosion product emerges from multiple pores in the epoxy near the diode ends and coalesces into a film with a constant thickness of 2µm and a width limited to 25% of diode circumference.
- The 2µm film spreads longitudinally across the diode surface from both ends until the diode is bridged.
- The film then spreads circumferentially, maintaining a thickness of 2µm until the entire surface is covered at which point the film thickens.

Of relevance to the integrated objective of this section, neither the porosity in the epoxy layer nor the initial concentration of sulfur species in the rubber bands is a single value, deterministic parameter. Rather, each is distributed with characteristics reflective of fabrication processes and starting materials. Their existence was incorporated into the simulations by using the CRAX software (and calculational framework) described in some detail in the Modeling Approach section. The first computational activity consisted of iteratively solving the equation set with CRAX using nominal storage conditions to compute distributions for both of these parameters with the criterion being to reproduce the actual diode failure characteristics observed after 5 years in storage. The resulting distributions (probability density functions) for these input parameters are shown in Figure 15.

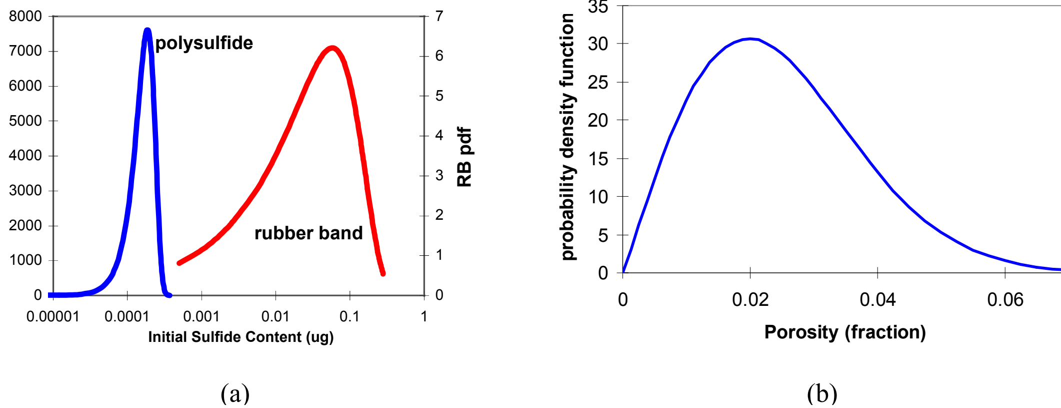

(a) (b)

Figure 15. Derived distributions of environmental (a) and physical (b) input parameters. In (a), the rubber band function is relevant to the storage environment while the polysulfide distribution is from a hypothetical deployment environment.

One useful application of this model is an assessment of the long-term effects of assembling circuits using previously sulfided (dirty) diodes. In this situation, the source of sulfur changes from rubber bands to a polysulfide-staking compound (possible distribution also shown in Figure 15(a)). Using the source term and product-layer growth characteristics defined above, CRAX-based simulations were performed in which the sulfide and porosity distributions were randomly sampled. Figure 16 shows the resulting distribution of electrical conductance as a function of time. At short times, the effect of using diodes that were previously sulfidized during storage is relatively significant. The population exhibits higher conductance and a larger fraction of the population is affected. At longer times the overall conductance has increased with the main contribution now being due to the exposure to the polysulfide, effectively swamping out the effect of using dirty diodes.

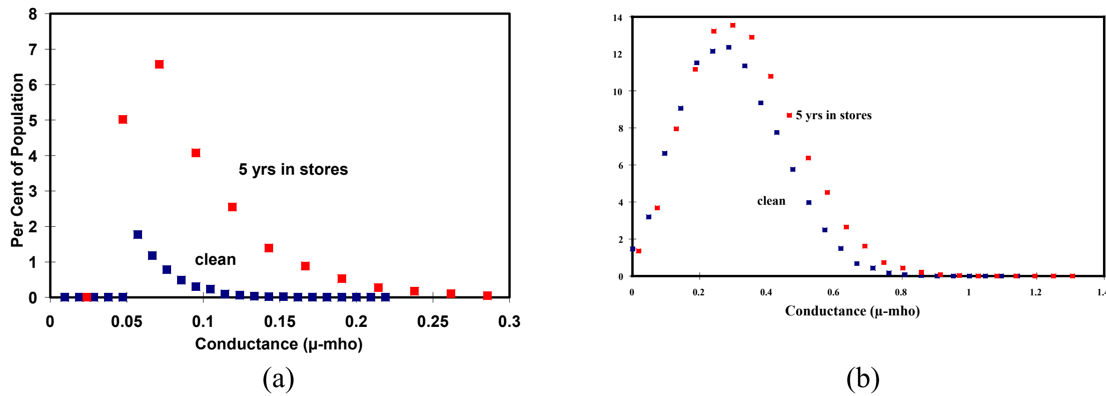

(a) (b)

Figure 16. Calculated conductance distributions for diodes in a hypothetical service environment containing gaseous sulfur species. Curves represent (a) short time and (b) long time exposure. The curves shown depict the effect of using sulfided diodes during component assembly.

The resulting distributions of conductance can then be used to directly calculate reliability for an electrical assembly by performing an age-aware circuit analysis. However, in cases when the circuit failure criteria are actually known, a simpler analysis is possible. In our first example, consider the diode-power OR circuit shown in Figure 17. Here the sulfide layer is modeled as a leakage resistor in parallel with the diode. The circuit output is a function of the load resistance (R_{load}), and is affected by the leakage resistance caused by the presence of the sulfide layer. Circuit failure occurs when the circuit output drops

below a minimum value (shown as the solid line in (b)). Combining the distribution of conductance values from the corrosion simulation with the circuit failure data shown in Figure 17(b) permits an estimate of failure probability to be made. For example, if the failure point for the response shown by the far right curve is used, a resistance greater than 2 k-ohms (or 500 μ-mho) is required. If the sulfidation response from Figure 16 is applicable, there would be practically no effect on reliability (500 μ-mho is well to the right of the possible values).

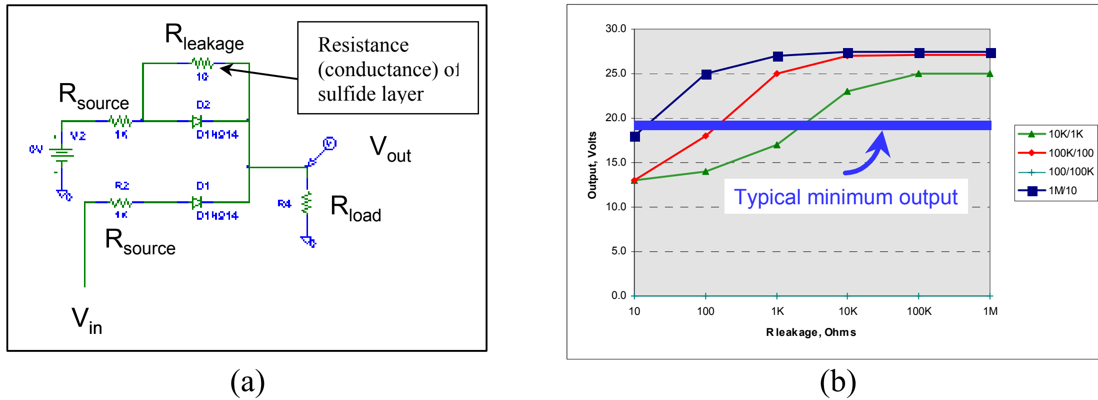

(a) (b)

Figure 17. Electrical system (diode power OR circuit) showing a leakage resistor to simulate copper sulfide on the diode surface. The plot in (b) shows the calculated electrical response with a criterion for failure.

Another way to perform a simpler reliability computation can be demonstrated with a second example that involves a simulation of the effect of diode sulfidation on the performance of a voltage regulator. Using this method, the critical diodes (those that affect most significantly affect circuit performance) along with their failure criteria are first identified by running a decoupled electrical circuit simulation. Then, a similar evaluation is conducted as that used in the previous diode power-OR circuit example. For this voltage regulator situation, output from a SPICE model simulation identified a critical diode in the circuit (see Figure 18). When the leakage conductance exceeds a value of 6,700 μ-mho, the circuit fails. By again comparing this value to the distributions shown in Figure 16, it is evident that the conductance values produced through the sulfidation process are several orders of magnitude lower than the critical value, indicating that corrosion (sulfidation) of the diode in this circuit would not be expected to adversely affect system reliability.

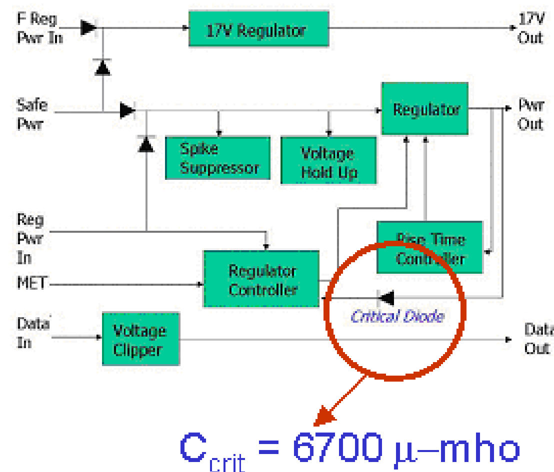

Figure 18. Voltage-regulator circuit showing location of the critical diode and the reverse-bias conductance (C_{crit}) value that results in circuit failure.

Aluminum Wirebond Corrosion

In contrast to the two simplified examples just discussed, the full implementation of this toolset consists of combining the deterministic model with uncertainty analysis to compute time-based distributions of corrosion-induced changes in an electrical property. These distributions are then directly input into an age-aware circuit simulator. An example of this integration is described in this subsection. Here, simulations are described of the effect of wirebond corrosion on the reliability of plastic-encapsulated microelectronic devices. In our applications, the primary concern involves corrosion during long-term dormant (unpowered) storage. In this situation, sufficient time exists to permit equilibration with external environment and degradation mechanisms associated with electrical bias (e.g., electromigration, electrolytic dissolution, cathodic corrosion) are not relevant.[13,14]

Wirebond degradation was measured as a function of three prime environmental parameters: temperature (T), relative humidity (RH), and gaseous contaminant concentration ([Cl_2]). The gaseous contaminant was chosen as a simulant for atmospheric halogen species and potential off-gas species from the encapsulant. A special corrosion test chip was designed and used in a flowing gas exposure system to measure corrosion kinetics.[13] Each of these test devices contains eight identical sets of Au-Al wirebonds that permits standard four-point resistance measurements to be made. Our studies showed that the change in wirebond resistance is an effective metric for the extent of corrosion.[13]

Consideration of the kinetic data shown in Figure 19 led to the several observations. First, if the same rate data as shown in Figure 19(a) are plotted on a linear scale (Figure 19(b)), the response is generally linear with time up until the time of rapid wirebond failure (open circuit). Thus, under constant environmental conditions used in these experiments:

$$\frac{d(\Delta R/R_o)}{dt} = k \qquad (7)$$

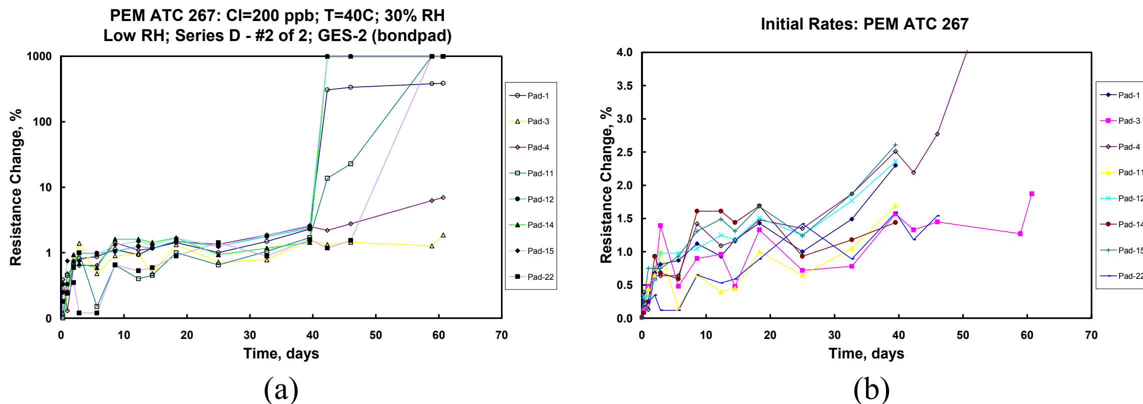

Figure 19. Typical wirebond corrosion data: resistance change data plotted as a function of time on a logarithmic scale (a), and the same data plotted on a linear resistance scale (b). The data in frame (b) show the relatively linear response with time. In frame (a), note that sudden rise in resistance that occurs above the ~10% level. Visual observation confirmed that this dramatic increase correlated with gross failure of the wirebond. The other interesting feature is the differences between the “identical”eight individual wirebonds on the test device.

Usually this “linear” response was seen when ΔR values are less than 10%. Such a linear rate would be consistent with control by a diffusion-limited transport process (e.g., oxidizing reactant through the gas or thin adsorbed water layer) and a small change in the interfacial area at which the heterogeneous

corrosion reaction is occurring. This latter factor could be easily satisfied given that the resistance change is limited to 10%. Based on some modeling work not reported here, we believe that the considerable scatter that exists in these rate data between the individual wirebonds is due to differences in the distributions of the intermetallic phases between the different wirebonds.[13] Other possible factors include unaccounted for geometric effects (e.g., bond location, water condensation, galvanic interactions) or possibly even the stochastic nature of the Al corrosion process itself.

The effect of chlorine concentration on wirebond corrosion is shown in Figure 20. It is clear that increasing the chlorine concentration increases the corrosion rate. The rate data for all of the experiments are compiled in Figure 20(b). There is a limiting value of [Cl_2] above which the rate no longer increases. For reference, data exist above 150 ppb but are not shown. Up to this limit, there appears to be a relatively linear relationship between chlorine concentration and the corrosion rate. This linear behavior is consistent with a first-order surface reaction or possible gas or liquid phase mass transport control. The 150-ppb limit may be due to a saturation effect (adsorbed water layer or surface) or a change in mechanism.

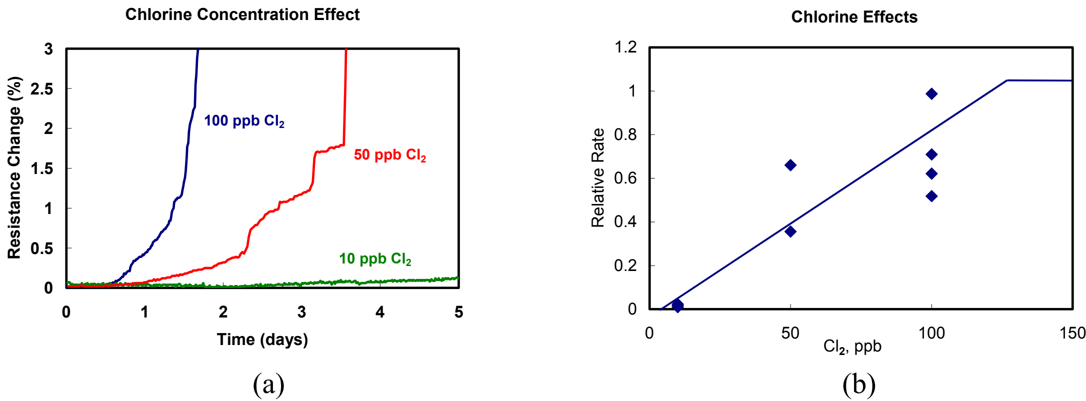

Figure 20. The effect of chlorine concentration on wirebond corrosion: (a) typical raw data and (b) resulting relationship.

Similarly, the effect of relative humidity is shown in Figure 21. Based on most atmospheric corrosion situations, the expected positive correlation between the relative humidity and corrosion rate was observed. The data (e.g., those shown in Figure 21(a)) were fitted to a sigmoidal curve that is also typically observed for atmospheric corrosion processes. Based on this response, the critical humidity for Au/Al wirebond corrosion is around 20% RH.

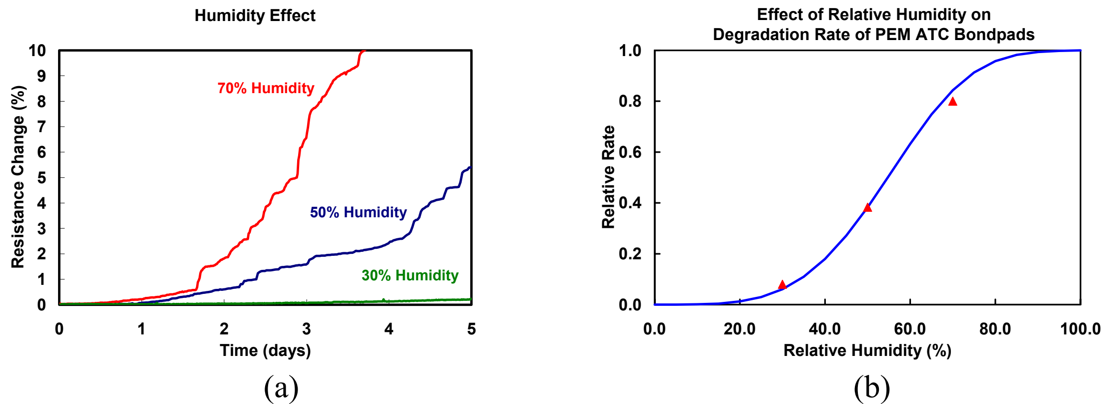

Figure 21. Effect of relative humidity on wirebond corrosion: (a) typical raw data and (b) resulting relationship.

To determine numerical values and parametric dependencies for the reaction rate constant (k) contained in Equation (7), the resistance change data up to 10% from all the kinetic experiments were analyzed. First, lumped rate constants were obtained by performing a linear regression on each set of wirebond data. Then, multi-variable analyses using all the lumped rate constants were conducted to identify the effect of chlorine concentration, temperature and relative humidity. This effort resulted in the following deterministic equation for wirebond corrosion:

$$\frac{d(\Delta R/R_o)}{dt} = k_o P_{Cl_2}\left\{1-\exp\left[-\left(\frac{H}{\eta}\right)^{\beta}\right]\right\}\exp\left[-\frac{E_a}{RT}\right] \tag{8}$$

where $\Delta R/R_o$ is the change in wirebond resistance, k_o is the surface reaction rate constant, P_{Cl_2} is the concentration of gaseous chlorine, H is the relative humidity, E_a is the activation energy, and T is the temperature. The specific values for each of the parameters are the following: β=2.5, η=55, E_a = 0.8 eV or 17.5 kcal/mole. Of note, the activation energy is completely consistent with other investigators measurements of this parameter.[14]

One source of uncertainty in Equation (8) is the variability in the temperature and humidity environmental parameters that generally change with time. To include these distributed parameters in the simulations, environmental data were collected and analyzed for three locations: nominally arctic (Fairbanks, AK), desert (Albuquerque, NM) and gulf coast (Houston, TX). Weather service data consisting of 65-year averages for the three locations were obtained (Figure 22). As can be seen in the figures, the data follow a very sinusoidal relationship. An analysis was then performed using these data and associated additional data containing daily extremes in T and RH that resulted in the following simple functions:

$$H(t) = \left[\mu_h + A_h \sin\left(\frac{2\pi t}{f_h} + \delta_h\right)\right] + \varepsilon_h \tag{9}$$

$$T(t) = \left[\mu_T + A_T \sin\left(\frac{2\pi t}{f_T} + \delta_T\right)\right] + \varepsilon_T \tag{10}$$

where μ_i, A_i, f_i and δ_i are deterministic parameters that describe the average monthly humidity at each specific location. The parameter ε_i is a Gaussian distributed random variable with zero mean and known coefficient of variation that captures the variability in the daily temperature and humidity. Values for each of these parameters are shown in Table 2 and Table 3. Of note, these data and equations are representative of outdoor conditions. Thus, the simulations that follow would be more representative of outdoor-type applications (e.g., dormant storage in non-hermetic containers). However, thermal and moisture transport calculations involving the plastic encapsulant showed that the conditions at the inner die surface quickly (within hours) equilibrate with the external environment.[13] Therefore, in the case of plastic packaged microelectronics, a very reasonable assumption is to use the external temperature and humidity as representative of what would exist on the bondpad itself.

A second source of uncertainty in Equation (8) is the surface reaction rate constant, k_o. As seen in Figure 19, considerable scatter exists in the data for any given experiment. Values of k_o were determined for each wirebond, producing a population with a mean value and standard deviation. Another needed modification to the deterministic model involves the physical integrity of the plastic-encapsulation. As described above, this layer has little effect on moisture or heat transport. However, when a good physical bond between the plastic and the wirebond exists, it can effectively prevent any environmental

interaction. Therefore, by making the justified assumption that corrosion will only occur within physical defects in the plastic, a simple addition of a defect identity function (*I*) term can be included. The identity function takes on values of either 0 or 1 that are allocated based on an assigned probability. The governing equation describing the kinetics of wirebond corrosion now has the following form:

$$\frac{d(\Delta R / R_o)}{dt} = I(defects)k_o P_{Cl_2}(t)\left\{1 - \exp\left[-\left(\frac{H(t)}{\eta}\right)^{\beta}\right]\right\}\exp\left[-\frac{E_a}{RT(t)}\right] \qquad (11)$$

This equation contains five distributed parameters: I, k_o, P_{Cl2}, $T(t)$ and $H(t)$. As indicated, three of these variables (T, H, and P_{Cl2}) are, in general, also time dependent.

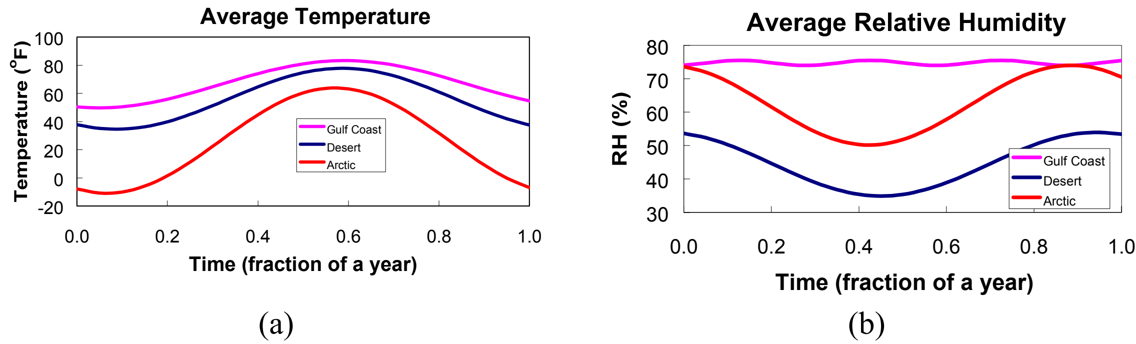

Figure 22. Environmental data used for simulation. Data represent 65 year averages for three locations (Fairbanks, AK, Houston TX., and Albuquerque, NM.).

Table 2. Parameters describing temperature distributions

Location	μ	A	f	δ	ε
Fairbanks, AK	-3.06	20.78	1.01	4.31	12.0
Houston, TX	19.17	9.32	1.09	4.44	8.0
Albuquerque, NM	13.47	12.01	1.00	4.17	9.0

Table 3. Parameters describing humidity distributions

Location	μ	A	f	δ	ε
Fairbanks, AK	62.10	11.92	0.92	1.83	3.0
Houston, TX	74.74	0.00	0.29	5.15	7.5
Albuquerque, NM	44.44	9.54	0.16	0.52	7.0

Using Equation (11), which contains non-deterministic distributed parameters, two simulations of electrical circuits were performed. Both of the simulations used a common set of values for these random parameters. For those that are not time dependant, the following values were used:

- All of the values derived for k_o were analyzed and found to follow an empirical log-normal distribution with mean and coefficient of variation = 1.77×10^{13} and 0.517 respectively. The mean value has the units of percent/ppb-year. As such, the units for each of the parameters in the governing equation are as follows: $[Cl_2]$ = ppb, RH = %, T=°K and time=years. The integration of the equation will then output ΔR/R as a percent change.
- The chlorine concentration (P_{Cl_2}) was fixed at a relatively low value of 0.01 ppb. This concentration was conservatively and loosely based on measured tropospheric levels of potentially more corrosive HCl that range from 0.1 to 0.3 ppb.[15]

- Based on our examination of several commercial PEM devices using scanning acoustic microscopy, we estimated that the identity function (I) should have a probability that a critically sized defect exists above a wirebond of about 3%.

The initial computation that was performed involved calculating the resistance response of a single corroding wirebond during exposure to the Albuquerque "desert" environment. The results are shown in Figure 23 as a cumulative distribution function for the ΔR/R parameter. Once these distributions of resistance values were generated, the data were inserted into the appropriate electrical circuit model. The first circuit simulation was run to model the effect of wirebond corrosion on the reliability of a voltage comparator. Figure 24 is a schematic diagram of the comparator, a simple electrical circuit that monitors the voltage differential between two outputs. Three transistors in the circuit are PEM parts with Au-Al wirebonds. The circuit maintains a tolerance level on the voltage difference over the operational period of the circuit (approximately 500 ms).

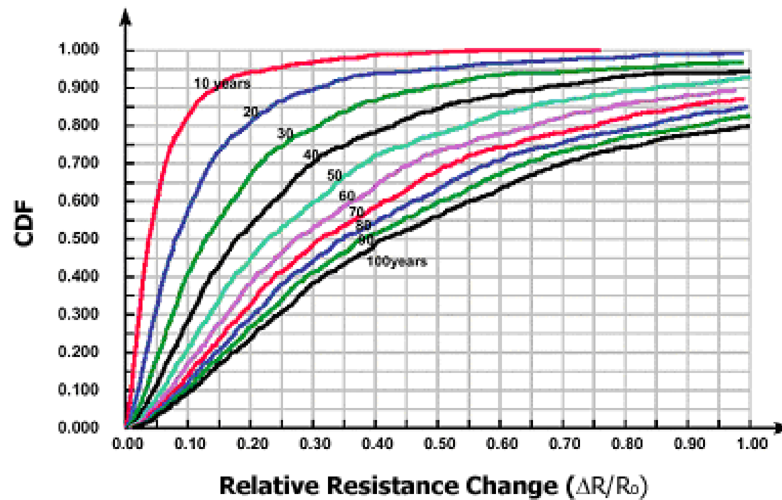

Figure 23. Cumulative distribution functions (CDF) of the relative change in wirebond resistance as a function of aging time due to corrosion in the

Corrosion of each wirebond was modeled as a resistor in series with the associated lead wire (small resistors in Figure 24). As the comparator ages, the wirebond resistance increases according to relevant distributions of responses from the corrosion model (Figure 23). The modified comparator circuit was evaluated using ChileSPICE that was linked directly to CRAX (Figure 8).

Figure 25 presents the time-based output from ChileSPICE and shows how the electrical performance of this circuit degrades with time. Each line represents the probability of the circuit performing within specifications over its 500ms operational requirement. As the system ages, the wirebonds corrode, significantly impacting the reliability of the circuit. Under these assumed conditions, after approximately 20 years, the circuit performance has decreased to the point where there is only a 90 percent chance that it will operate within the required specifications. After 40 years the probability of proper function has dropped to approximately 85 percent. These data are re-plotted as a time-based reliability curve in Figure 26.

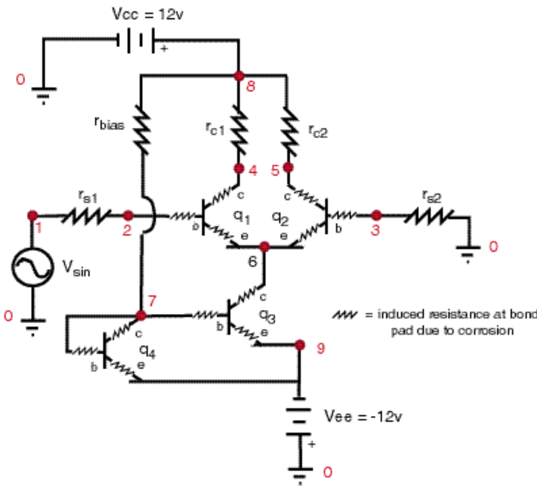

Figure 24. Schematic diagram of a simple voltage comparator device. Failure is determined through analysis of the entire electrical circuit.

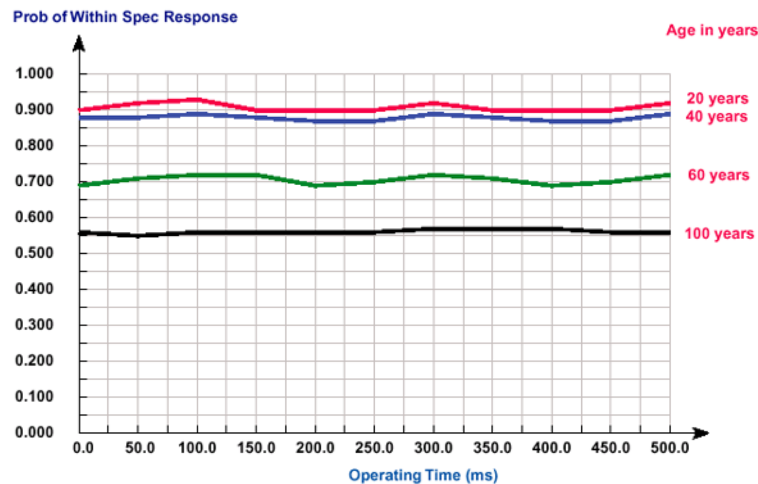

Figure 25. Comparator electrical system performance as a function of system age.

A second simulation was performed to show how the storage environment can affect device reliability and how these techniques permit effective parametric sensitivity studies to be performed. This aging simulation utilized the 3-lead LM185 voltage reference device previously shown in Figure 5. In this case, the wirebond failure criterion was conservatively chosen to occur when any of the wirebonds increased in resistance by 2%. For reference, the ChileSPICE simulation of this very robust device determined that the resistance of the most sensitive lead must actually increase by about 1 kΩ to cause device failure. The three environments described previously were used. The only contaminant was chlorine gas, whose concentration was again fixed at 0.01 ppb.

The effect of the external environment on device reliability is shown in Figure 27(a). The Gulf Coast clearly provides the most aggressive environment of the three considered. This is likely due to the relatively constant and high humidity and temperature encountered. Comparing the other two locations, an arctic exposure has a lower average temperature, but a higher relative humidity, while the desert has a higher temperature and lower humidity. The two effects countered each other and gave similar corrosion rates. In addition, informative parametric sensitivity studies were performed (Figure 27(b)) that showed how changes in environment and physical configuration can influence the computed reliability.

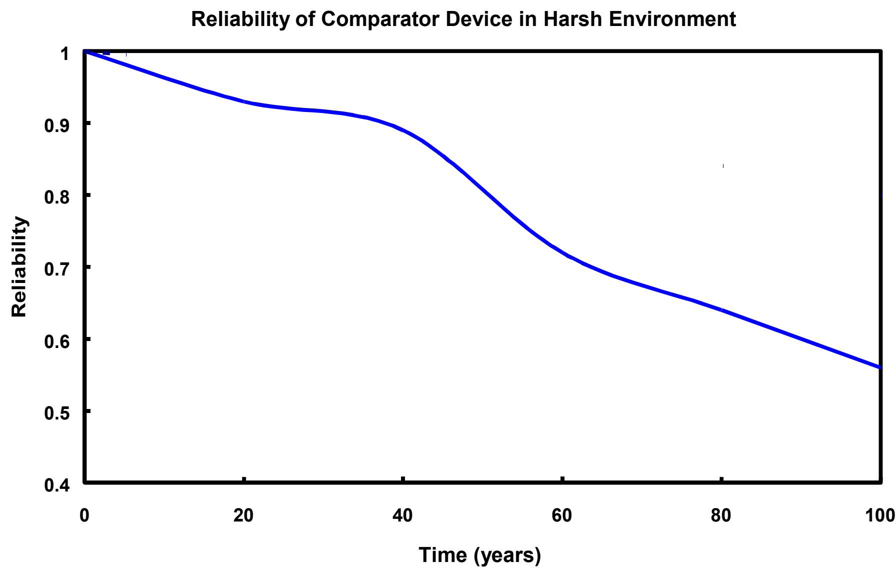

Figure 26. Predicted reliability of a comparator circuit and a hypothetical device with a single wirebond and for multiple wirebonds in the comparator circuit.

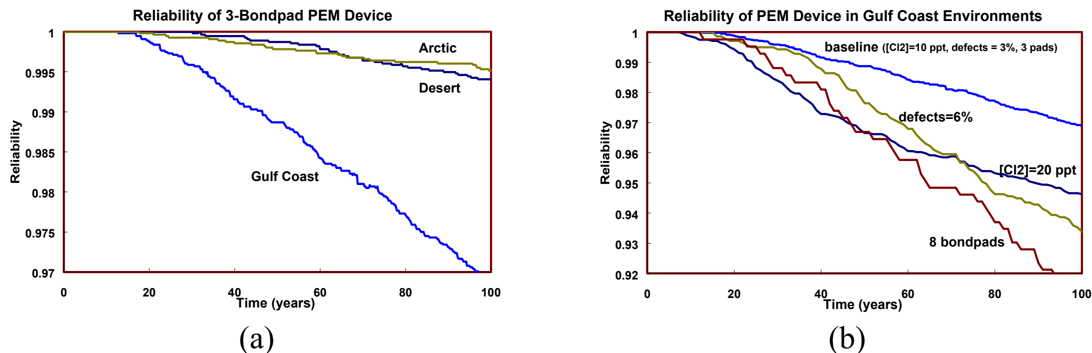

Figure 27. Results from the aging simulation of an LM185 voltage-reference device. In (a), the effect of environment is presented, while (b) shows how variations in environmental and physical parameters can affect reliability.

Summary

A clear need exists for having an analytical capability (computational toolset) that can be used to predict the effects of atmospheric corrosion on the long-term performance of electrical circuits and systems. Applications for this capability include aiding system and device-specific design, assessing consequences and remediation options for observed field failures, and determining the viability of extending product life. Sandia has adopted a statistical-based, top-down approach for developing an effective engineering-level capability. The prime benefit of the selected approach involves surmounting a number of significant development and implementation obstacles that certainly would prohibit the attainment of a fully rigorous and science-based capability. Nevertheless, executing our selected approach is still a formidable undertaking because a number of diverse requirements must be incorporated in a very computationally efficient framework. Some of these challenging aspects include:

- Identifying and maintaining a mathematical linkage between critical aspects dealing with scientific understanding for a wide range of potentially relevant degradation modes all the way up to the electrical-circuit models,
- Maintaining flexibility to enable an enormous number of devices and system configurations to be included, and
- Addressing the existence of non-deterministic (uncertain) modeling parameters.

Work on the development of this capability is currently underway at Sandia. Two specific types of corrosion degradation were selected to use as the vehicles to enable advances to be made: sulfidation of copper-containing features (e.g., in diodes, contacts, connectors) and voiding of thin-film aluminum in Au-Al integrated-circuit wirebonds. The progress made to date highlights many aspects of this top-down approach and has already demonstrated the ultimate usefulness of such a toolset.

Acknowledgments

The authors would respectfully like to acknowledge the contributions several other collaborators have made to the work reported in this paper including Samuel Lucero, Charles Barbour, David Peterson, James Sweet, Bonnie McKenzie, and Joseph Michael.

References

1. http://www.seas.upenn.edu/~jan/spice/spice.overview.html.
2. Gelman, A., J. Carlin, H. Stern, D. Rubin, Bayesian Data Analysis, Boca Raton, Chapman and Hall/CRC, 2000
3. D. Robinson, "Hierarchical Bayes Approach to System Reliability Analysis," SAND2001-3513, Sandia National Laboratories, Albuquerque, NM, November 2001.
4. D. Robinson, "An Application of Bayesian Methods for Combining Data from Different Test Modalities Hierarchical Bayes Approach to System Reliability Analysis," SAND2002-3953, Sandia National Laboratories, Albuquerque, NM, December 2002.
5. http://reliability.sandia.gov/crax
6. D. Robinson, C. Atcitty, "Comparison of Quasi- and Psuedo-Monte Carlo Sampling for Reliability and Uncertainty Analysis," AIAA 99-1589, AIAA SDM Conference, St. Louis, MO, April 1999.
7. D. Robinson, "Application of Spatial Statistics in Characterizing Structural Reliability and System Uncertainty," SAND99-2055, Sandia National Laboratories, Albuquerque, NM, August 1999.
8. http://www.corba.org/
9. J. C. Barbour, et.al., "Mechanisms of Atmospheric Copper Sulfidation and Evaluation of Parallel Experimentation Techniques," SAND2002-0699, Sandia National Laboratories, Albuquerque, NM, March 2002
10. T. E. Graedel, J. P. Franey, and G. W. Kammlott, "The Corrosion of Copper by Atmospheric Sulfphurous Gases," *Corrosion Science*, **23** (11), 1983, pp. 1141-1152.
11. T. E. Graedel, et. al., "On the Mechanism of Silver and Copper Sulfidation by Atmospheric H_2S and OCS," *Corrosion Science*, **25** (12), 1985, pp. 1163-1180
12. K. Okamoto and S. Kawai, "Electrical Conduction and Phase Transition of Copper Sulfides," Japanese Journal of Applied Physics, **12** (8), 1973, pp. 1130
13. N. R. Sorensen, J. W. Braithwaite, S. J. Lucero, J. R. Michael, J. N. Sweet, D. W. Peterson, D. G. Robinson, K. L. Erickson, and C. C. Battaile, "Physical Models for Predicting the Effect of Atmospheric Corrosion on Microelectronic Reliability" SAND2000-3008, Sandia National Laboratories, Albuquerque, NM, December 2000.
14. G. S. Frankel and J. W. Braithwaite, "Corrosion of Microelectronic and Magnetic Data-Storage Devices," Chapter 15 in *Corrosion Mechanisms in Theory and Practice*, 2nd edition, P. Marcus and J. Oudar, ed., Marcel Dekker, Inc., New York, 2002
15. T.E. Graedel and W.C. Keene, "The Budget and Cycle of Earth's Natural Chlorine," *Pure and Appl. Chem*., **68** (9), 1996, pp. 1689-1697

Distribution

1	MS 1415	J. C. Barbour, 1112
1	MS 1415	M. J. Campin, 1112
1	MS 1415	K. Leung, 1112
1	MS 1415	N. A. Missert, 1112
1	MS 1415	J. P. Sullivan, 1112
2	MS 0525	C. W. Bogdan, 1734
1	MS 0525	P. V. Plunkett, 1734
5	MS 0889	J. W. Braithwaite, 1832
1	MS 0888	D. G. Enos, 1832
1	MS 0888	S. J. Lucero, 1832
5	MS 0888	N. R. Sorensen, 1832
1	MS 0888	F. D. Wall, 1832
1	MS 1411	S. M. Foiles, 1834
1	MS 0889	R. J. Salzbrenner, 1835
1	MS 0750	L. J. Criscenti, 6118
1	MS 0750	R. T. Cygan, 6118
2	MS 0748	D. G. Robinson, 6413
1	MS 0748	R. D. Waters, 6413
2	MS 0834	K. S. Chen, 9114
1	MS 0834	J. E. Johannes, 9114
1	MS 0834	H. K. Moffat, 9114
1	MS 0834	A. C. Sun, 9114
1	MS9018	Central Technical Files, 8945-1
2	MS0899	Technical Library, 9616
1	MS0612	Review and Approval Desk, 9612 for DOE/OSTI